JOURNAL OF AIRCRAFT
Vol. 35, No. 1, January–February 1998

Deflection of Turbofan Exhaust Streams for Enhanced Engine/Nacelle Integration

R. H. Tindell* and F. Marconi*
Northrop Grumman Corporation, Bethpage, New York 11714
I. Kalkhoran†
Polytechnic University, Farmingdale, New York 11735
and
J. Yetter‡
NASA Langley Research Center, Hampton, Virginia 23681

An analytical and experimental description of how the fan exhaust of a modern turbofan can be deflected into an annular cascade using only core bleed flow is presented. Thrust reversing, emphasized herein, and/or vectoring is achieved without the need for fan duct blockers or other hardware devices to turn the flow, allowing lighter, less complex, and lower loss exhaust systems for more efficient up-and-away flight. Two approaches for deflecting fan flow into an annular cascade, using two different models, are described, and test results are discussed. Results of a Euler analysis and its critical relationship with the testing are also described. Both methods use injected core flow to turn the fan flow. One method uses an annular air-curtain emanating from an annular injection slot located opposite the cascade and the other uses a similar slot in the nozzle throat to force upstream flow into the cascade. Both approaches are impacted by engine core bleed limits. Injector jet arrangements to meet this requirement while providing adequate reverse thrust are described; analyses and test results are reviewed.

Nomenclature

A = area, in.^{2}
BPR = bypass ratio
F = axial thrust, lb
FPR = fan pressure ratio, Pt_f/P_a
H = height of annular duct at upstream end of translating cowl, in.
L = distance between injector jet and upstream end of translating cowl, in.
M = Mach number
Pa = ambient pressure, psia
Pt = total pressure, psia
R = radius, in.
S = cascade opening, in.
TR = thrust reverser
t = injection slot exit thickness, in.
W = flow rate, lb/s
X = axial distance, in.
Y = vertical distance, in.
ϕ = angle of injector jet above local surface, deg

Subscripts
b = bleed
c = core
f = fan
fwd = forward thrust operation (stowed cascade case)
i = injection slot
lip = location of upstream corner of translating cowl
noz = forward thrust nozzle
rev = reverse thrust operation (deployed cascade case)
s = cascade opening
0 = freestream

Received Dec. 7, 1996; revision received June 26, 1997; accepted for publication June 26, 1997.

*Principal Engineer, Advanced Systems and Technology. Associate Fellow AIAA.
†Associate Professor of Mechanical Engineering and Aeronautics. Member AIAA.
‡Research Engineer, Component Integration Branch.

Introduction

CURRENT state-of-the-art cascade thrust reverser systems require mechanical blockers to close off the fan duct and divert the fan flow outward and forward through a set of cascade vanes. These blockers sustain high loads, are heavy, and result in performance losses caused by pressure drops and leakages when in the stowed (in-flight) position. Although the reverser system is used for only a small fraction of the airplane operating time, its impact on nacelle design, weight, cruise performance, engine maintenance, and aircraft operating expense is significant. NASA investigations[1] have shown that the thrust reverser system can account for more than 30% of the nacelle weight (not including engine) for an engine having a fan diameter in excess of 100 in. This can be as much as 1500 lb for a GE 90 class engine. In addition, the reverser system has been estimated to increase engine specific fuel consumption (SFC) by 0.5–1.0% because of leakage and pressure losses. The cost for use of typical thrust reversers has been estimated to be $125,000 per aircraft per year.

The blockerless engine thrust reverser (BETR) concept is aimed at providing reverse thrust without a mechanical blocking device and its hardware, thereby offering a lighter, more efficient reverser system for in-flight performance, with reduced operating and maintenance costs. The BETR concept is shown in Fig. 1a. It employs injected engine core flow to separate the fan flow from the core housing and block the fan duct, thus deflecting the flow outward through the cascade vanes. No movable blocker panels and linkages are necessary. Exhaust duct pressure losses incurred by blocker door links in up-and-away flight are eliminated in the BETR. The most significant design issue is the arrangement of the nozzles (annular slots) used to inject the core bleed flow into the fan stream. The number of injection slots, their location, size, and direction

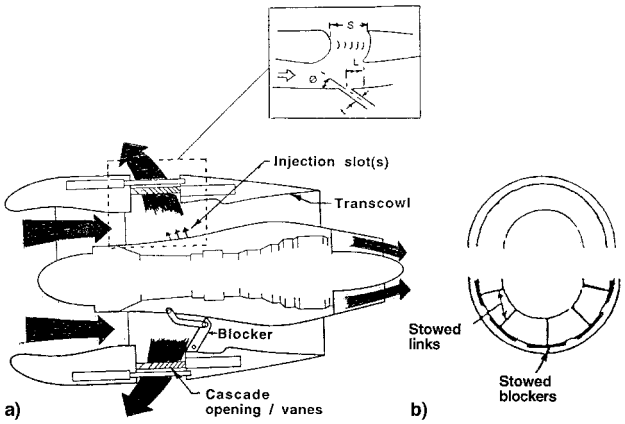

Fig. 1 Blockerless thrust reverser concept: a) cross-sectional view and b) view of stowed reverser ducts looking forward.

can be critical to the ability to separate the fan flow from the core wall and turn into the cascade with small amounts of core bleed flow.

To evaluate these concerns and demonstrate the concept's validity, Northrop Grumman Corporation (NGC) has teamed with the NASA Langley Component Integration Branch (CIB) to conduct analytical and experimental investigations. Each team member has developed a BETR experimental model, the NGC model being specifically designed to fully explore BETR parametrics, whereas the NASA model is a limited experimental modification of an existing thrust reverser rig. Initial testing of the NGC model, which first demonstrated reverse thrust capability for the BETR concept, albeit at relatively low simulated fan operating conditions, has been performed and is reported in Ref. 2. The NGC and NASA testing periods for the present work, which thoroughly explored system parametrics, are presented herein.

Concept Definition

The BETR concept is based on the integration of two innovative exhaust system fluidic techniques that have been postulated and published for more than 30 years. For example, Ref. 3 described the concept of bisecting and deflecting a round propulsive jet in opposite directions using two small high-pressure injector jets emanating from a spanwise fairing that transversed the diameter of the propulsion jet. The injection station was immediately upstream of a set of turning vanes and caused the exhaust flow to separate into two opposite streams. This approach relied upon a complementary Coanda-like effect occurring on an external (contoured) base area upstream of the propulsion nozzle to assist in inducing the flow to turn. The BETR approach uses annular injector jets, emanating from the inner (core) surface of the fan duct, opposite the annular turning vanes, to emulate the curtain jet described in Ref. 4. This approach requires the injection flow to separate the fan flow from the core surface as in the approach of Ref. 3, and, if the injection slot is appropriately configured, to force the fan flow outward into the cascade vane slot. The applicability of the air curtain concept to turbofan thrust reversing, i.e., that a small thin annular jet of high-pressure air can deflect a large fan stream into a cascade of reverser vanes, must be proven and constitutes the primary goal of the research to be described.

The concept described in Fig. 1a shows an annular fan exhaust with a translatable afterbody in an aft deployed position, and a vane cascade located in the resulting annular slot. The injection slots emanating from the core surface are fed core bleed air from a high-pressure compressor stage. They may be located opposite the cascade, as shown in Fig. 1a, and/or downstream near the throat. Each of these locations allows a different approach for causing the fan flow to turn into the cascade. The upstream location allows the air curtain approach, which causes the annular jet (curtain) emanating from the injection slot to impinge upon the inner surface of the fan stream, thus making it separate and leave the surface. If enough momentum can be brought to bear by appropriately configuring the injector jet, then the fan and injected flows may be turned into the cascade opening. The downstream location, with the injection slot located near the nozzle throat, allows the injected flow to restrict or block the flow through the nozzle section, causing a back-pressure that will turn the fan flow into the cascade opening. The inset in Fig. 1a defines the primary geometric parameters investigated herein: S, t, L, and ϕ. An axial view up the fan ducts of both a conventional installation and a BETR installation (Fig. 1b) shows the aerodynamically cleaner configuration of the latter.

Reference 4 describes the trajectory of a two-dimensional jet penetrating into a uniform crossflow at various angles to the surface and provides an analytically crude but useful means for preliminary evaluation of some BETR problems and solutions. Figure 2 shows results of such an analysis, describing the benefits of directing the jet upstream. The example is based on the assumption that locating the impingement point either at or above the inner corner of the afterbody, point P, will deflect the fan stream into the cascade opening. This analysis suggests that the angle between the injector location and point P should be kept small to preclude large core bleed flow requirements. It shows that an injection flow of 4% of the fan flow, $W_i/W_f = 0.04$ at $\phi = 90$ deg, does not provide enough penetration, and the injected flow passes through the nozzle. The analysis also shows that increasing the injected flow by 50% or directing the smaller stream forward at $\phi = 60$ deg will move the impingement point forward to point P. The latter case, of course, is the desired approach. The upstream-directed injection flow approach will be shown to be qualitatively validated by Euler computational fluid dynamics (CFD) analysis and experimental results. The Euler analysis also will show that the flow mechanics are much more complicated than the formulation shown in Ref. 4.

The second approach, with the injector jet located in the throat favorable static pressure gradient, allows the blowing to restrict or block the flow through the nozzle, thereby causing a strong adverse pressure gradient that will turn the fan flow into the cascade. Investigation of the throat-blowing approach is one of the major goals of the research reported herein.

In practice, there will be limits on the amount of core bleed available, depending upon the engine bypass ratio. For example, if an injection flow ratio of $W_i/W_f = 0.03$ is required for BETR operation in an engine with bypass ratio of BPR = $W_f/W_{\text{core engine}} = 9$, it would be necessary to bleed 27% of the core engine flow. Because this would affect the thrust available for reversing, it is clear that very low core bleed flow requirements as well as highly integrated engine–airframe integration

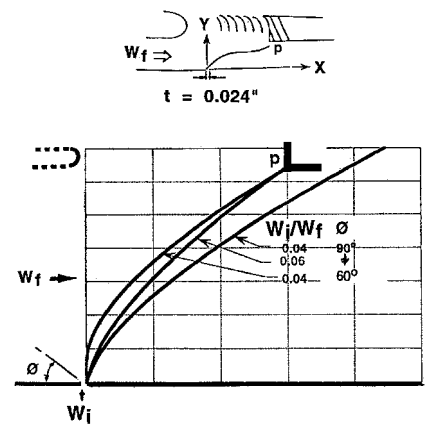

Fig. 2 Curtain jet simulation of annular injection jet.

will be required. Note that the inverse of the W_i/W_f value can serve as a figure of merit for being able to turn the fan flow into the slot with a minimum amount of core bleed flow, i.e., 33.3% of fan flow turned for each 1% of core bleed flow.

Model Descriptions

Two subscale models simulating annular-fan exhaust systems were developed to evaluate the BETR concept under static operating conditions. The NGC model was designed to allow a broad evaluation of geometric parameters that could influence BETR reverser performance. This model, although axisymmetric, was configured to approximate a CFM 56 turbofan engine installation, which has a bypass ratio of approximately BPR = 5. It was designed and tested at NGC and at the Polytechnic University. The NASA model is the NASA Langley Innovative Thrust Reverser Rig, modified to evaluate the BETR concept and to allow parametric evaluation of various geometric parameters. It approximates a BPR = 9 turbofan exhaust system installation. It is important to note that there is no implication that the two models represent reverser exhaust configurations driven purely by engine bypass ratio. Most significantly, the two model configurations reflect different usage goals, the NASA goal being to evaluate many diverse reverser design approaches, and the NGC goal to maximize geometric variability for a single baseline arrangement.

A comparison of the two models is made in Fig. 3, with a summary of important geometry parameters given in Table 1. Notice that the ratio of stowed thrust reverser nozzle area to fan area is similar for both models, reflecting the similarity of fan pressure ratio of the two engines. Significant differences are the greater fan duct height and the smaller cascade opening of the NASA model. Both models have annular injection slots located opposite the cascade opening and the capacity to direct them at various angles to the core surface. The NASA model also has a downstream injection slot located at the nozzle throat. Each model has one vane cascade, the NASA model's

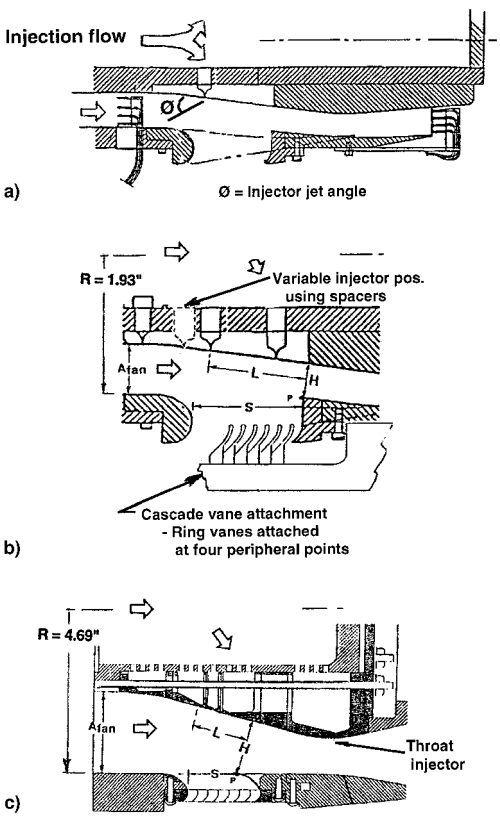

Fig. 3 Comparison of models: a) general arrangement, b) NGC model, and c) NASA model.

Table 1 Summary of geometry parameters

Injector position	NGC model			NASA model		
	Mid			Forward	Mid	Aft
S, in.	3	2	1.5	1.5	1.5	1.5
L/H	2.9	1.6	1.0	1.2	0.9	0.6
A_s/A_{fan}	3.5	2.3	1.8	1.2	1.2	1.2
A_{vane}/A_{fan}	2.8	1.6	1.2	0.61	0.61	0.61
A_{noz}/A_{fan}	0.73	0.73	0.73	0.68	0.68	0.68

being tailored to the single cascade opening of S = 1.5 in., and the NGC model's being adjustable to several openings. The NASA model's ratio of vane area to fan area is half the minimum value for the NGC model, reflecting the original design philosophy for this model. Also, the NASA model's vanes are relatively thin and reflect NASA reverser vane modeling philosophy. Oversizing of the vane exit area and relatively generous vane contours were provided for the NGC model, attempting to desensitize the system's performance to these elements for this preliminary testing. Baseline reverse thrust performance, for comparison with the BETR configuration's results, was obtained with the NASA model configured with a full (solid) blocker.

The importance of minimizing the angle between the injector jet and point P to allow small core bleed flow requirements for turning the fan flow into the cascade was pointed out in the previous section. Therefore, the cotangent of that angle L/H may be an important marker of performance potential and is noted in Fig. 3 for the various configurations. The L/H variation shown for the NGC model corresponds to the middle injection slot and three cascade openings (outer afterbody slides axially), while that of the NASA model corresponds to the three centrally located injectors and a fixed cascade opening.

Forces and moments for both models were measured with three-component balances. They were corrected for balance interactions and air system pressure and momentum tares determined from calibration runs. These calibrations ensured that 95% of the force data were correctable to within 0.5% of the balance full-scale load.

Each model has separate venturi measuring systems for fan and core flows. The NGC model flow measuring accuracy was within 2% over the operating range, and the NASA model's accuracy was within 0.10% over the operating range. Total pressures across each simulated fan discharge plane were measured with four-probe rakes that had outer wall statics at the probe leading-edge stations. The NGC model had two rakes, 180 deg apart, and the NASA model had three rakes approximately equally spaced. Each model also had four-probe total pressure rakes at the exit of the fan nozzle, data from which were used to calculate nozzle exit flow during reverser operation. A typical data run was performed by setting a desired fan flow or fan pressure ratio (with zero injection flow), and then systematically increasing injection pressure in discrete steps. Injection and fan flows were determined from their respective calibrated measuring systems, and nozzle exit flow was determined by integrating the nozzle exit rake data. Cascade flow was determined by subtracting nozzle exit flow from fan plus injection flow. Fan back-pressure characteristics were determined by the fan pressure increase required to maintain a desired level of fan flow, as injection pressure was increased.

It is useful to consider the basic exhaust systems' flow characteristics without blowing, which describe the operating environments within which the reverse thrust system must operate. Figure 4 shows the fan discharge total pressure ratio Pt_f/P_a, plotted against specific fan airflow rate W_f/A_f, for both models. Although the NASA model has a higher maximum fan pressure ratio, both models have similar pressure vs flow rate characteristics for the stowed cascade case. They both

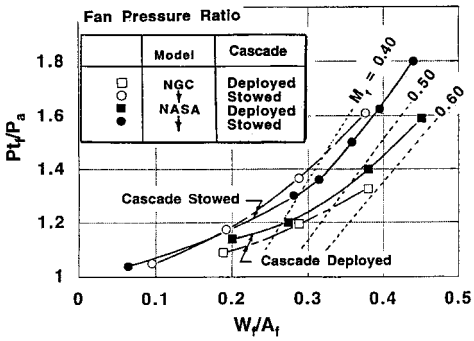

Fig. 4 Model operating characteristics without injection.

have a fan exit Mach number approximating $M_f = 0.44$ at high-power operation. It is assumed that reverse thrust operation, in the deployed-cascade mode, is required at specific airflows corresponding to the stowed-cascade fan pressure ratios, i.e., at higher fan exit Mach numbers than in the forward thrust mode. This implies that the engine must be capable of acceptable operation and of providing the required core bleed flow at the overspeed condition, which must subsequently be validated for each specific engine. Also, it will be necessary to ensure that any fan back-pressure effects caused by injection flow will be sufficiently small as to preclude an overloaded fan, i.e., fan pressures higher than the stowed cascade case.

CFD Approach

The CFD code used here to analyze NGC model performance employs second-order upwind difference operators to approximate spatial derivatives in the full Reynolds-averaged Navier–Stokes (FRANS) equations. The unsteady FRANS are integrated in time to asymptote to a steady flow. In the present application, only the inviscid terms are included, thus defining a Euler calculation, and the flow is assumed axisymmetric. These assumptions resulted in a simple/fast grid generation and turnaround time of about 2 h on an IBM/590 workstation. The numerical scheme is designed for the accurate prediction of high-speed flows and included a flux limiter to minimize oscillations at large gradients like shocks and contacts. The lower-speed regime considered here has compressibility effects, so that the numerical scheme used was deemed appropriate. The external exhaust system flow could not be modeled at zero velocity because of numerical incompatibilities. A Mach number of $M_0 = 0.10$ was the minimum that could be used, maintaining a reasonable convergence rate to a steady state.

Figure 5 shows a typical NGC model grid topology and typical boundaries for which the flow is assumed to be axisymmetric. For clarity, every other grid line is shown and the grid is truncated in the X and Y directions. All the calculations used 63 horizontal and 150 vertical grid points. Curve $A-B$ is the lower surface of the bypass duct. Curve $C-J'$ represents the upper surface of the bypass duct, and $E-J'$ is the nacelle external surface. The cascade opening is bounded by the curves $F'-G'-I'-H'-F'$. The trailing edge of the forward cowl is defined by $C-F'-G'-E$ and the translating cowl by $H'-J'-I'-H'$. The trailing edge of the translating cowl is at J'.

A grid blanking scheme is used, whereby the grid points in the region $C-F'-G'-E$ are disconnected from all other points because they are located inside the forward cowl. The same procedure is used for grid points located inside the translating cowl $H'-J'-I'-H'$. Grid blanking involved zeroing all of the elements of the alternating direction implicit (ADI) influence matrix at these points, thereby computationally disconnecting grid points both above and below these surfaces. The scheme was very effective, adding flexibility to a single block code.

Flow tangency is imposed along $A-B$, $C-F'$, $F'-G$, $G'-E$, $H'-J'$, $J'-I'$, and $I'-H$. Characteristic-based boundary conditions (Mach number of $M_0 = 0.10$ and ambient pressure Pa) are used to prescribe the freestream flow on a vertical line above point E and a horizontal line above points G, I, and K. The fan flow (design point of $M_f = 0.50$ and $Pt_f/P_a = 1.60$, for example) at $A-C$ also is prescribed with characteristic-based boundary conditions. For the subsonic conditions in the freestream and at the fan face, the characteristic boundary conditions allow upstream-running waves to affect the settings so that both the freestream and the fan conditions are only nominal. The pressure is forced to recover to ambient on a vertical line far downstream of points D and B. The injected flow was assumed sonic so that all conditions could be prescribed without upstream-running waves. The injected mass flow was controlled by varying either the pressure Pt_i or the injection slot thickness t.

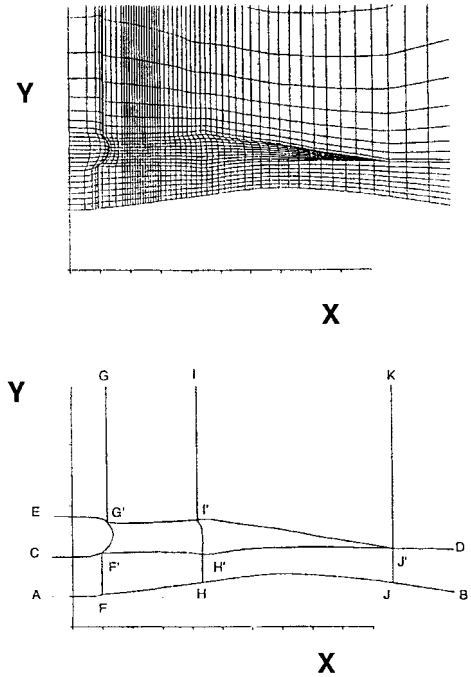

Fig. 5 Grid topology and boundaries.

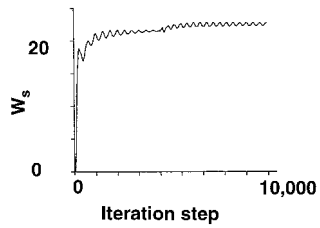

Fig. 6 Typical convergence history of cascade opening flow.

The convergence history of the iteration scheme does not show absolute convergence, i.e., the computation was unable to achieve machine zero. Convergence is monitored by observing the parameter of most importance, the weight flow out of the cascade slot W_s. Figure 6 is a typical plot showing the variation of cascade flow with numerical iteration step. It should be noted that the computation was approaching absolute convergence at 4000 steps when the differencing scheme was switched from first order to flux-limiting second order. This was done to increase reliability. The computation could be stabilized to achieve absolute convergence at the expense of spatial accuracy. It was decided that the uncertainties introduced by increasing the size of regions of first-order computation were too high a price to pay for absolute convergence. The maximum deviation at 9000 steps in the history plot of Fig. 6 is less than 2%.

Discussion of Results

Injector Jet Opposite Cascade

The effects of L/H on fan flow turning effectiveness for injector jets with $\phi = 90$ deg are shown in Fig. 7. The NGC model is without vanes installed. The ratio of flow in the cascade opening to fan flow is plotted against the ratio of injection flow to fan flow. These curves illustrate a number of interesting results. First, about 20% of the fan flow enters the cascade opening with zero injector flow. The addition of injector flow enables more fan flow to turn into the opening at about the same initial rate for the two lower L/H cases (1.03 and 1.63), and at a higher initial rate for the largest L/H, 2.88. When the cascade opening is filled with fan flow plus injected flow it is considered saturated, i.e., $W_s = W_f + W_i$, and further increases in injected flow add directly to the cascade-opening flow. Therefore, the slope of saturated cascade flow against injected flow is relatively flat, as shown in Fig. 7.

The NASA model was evaluated with vanes installed and its midinjector jet operating at an $L/H = 0.89$. The adverse effect of the lower L/H for the NASA model is roughly consistent with the L/H effects defined by the NGC model results, which show that excessive amounts of core bleed are required to turn the fan flow when L/H is approximately less than 1. The performance of the NASA model is roughly predictable from the trends of the NGC model results.

Notice that all of the configurations show an abrupt increase in the rate at which the cascade opening is filled after it is approximately half full. The Euler CFD model of the $L/H = 1.63$ configuration predicts the injected flow/cascade flow relationship rather well. This computational capability provided very useful and cost-effective problem solving and screening throughout the course of the program.

The results indicate the possibility of reducing injection flow requirements for filling the cascade opening with either a more forward location of the injector jet or a more aft location of point P, i.e., $L/H > 2.88$. Alternatively, results of the air curtain analysis (Fig. 2) suggest the possibility of reducing injection requirements by directing the flow upstream. Therefore, Euler CFD calculations were performed to evaluate the effects of injector angle on the NGC model.

Results of the Euler analysis of the NGC model without vanes installed are shown in Fig. 8. Recall that a freestream condition of $M_0 = 0.10$ is imposed to allow compatibility with the computational code. The fan operating condition is $W_f/A_f = 0.367$, and the injection slot flow ratio is held constant at $W_i/W_f = 0.02$. An 80% increase in cascade-opening flow, $\Delta W_s/W_f = 0.38$, is predicted when the injection angle is decreased from $\phi = 90$ to 35 deg. The streamline pictures show the large vertical deflection of the fan stream caused by reducing the injector angle. The larger cascade flow results from simultaneous deflection of the fan flow and constriction of the downstream nozzle duct by the vortical bubble. Other calculations have shown the same result when small increases in injected flow were imposed with a fixed injection angle. This explains the mechanism that drives the rapid increase in cascade flow with certain values of injection flow that is observed for all the configurations evaluated.

This mechanism, caused by the injection flow–fan flow–surface interaction, approximates a vortex valve powered by small amounts of injection flow. Because the vortex valve's deflection and constriction characteristics may be influenced by viscous effects, which are not simulated in the Euler calculations, a better understanding of the underlying physics may be provided with a Navier–Stokes analysis. Nevertheless, the Euler analysis is clearly capable of describing BETR flow mechanics sufficiently well for predicting trends and preliminary estimates of performance.

Experimental verification of the computationally predicted benefits of an upstream injector angle, although at lower fan flows and with a larger cascade opening, is shown by the data in Fig. 9 for configurations without vanes installed. Comparison of the $\phi = 90$ and 35-deg cases at $W_i/W_f = 0.02$ shows an improvement of $\Delta W_s/W_f = 0.43$ for the lower angle case. This agrees reasonably well with the Euler prediction of $\Delta W_s/W_f = 0.38$ (Fig. 8). The rapid rise in cascade-opening flow occurs at a lower injected flow and is at a steeper rate for the $\phi = 35$-deg case. In fact, the injection flow required to turn all the

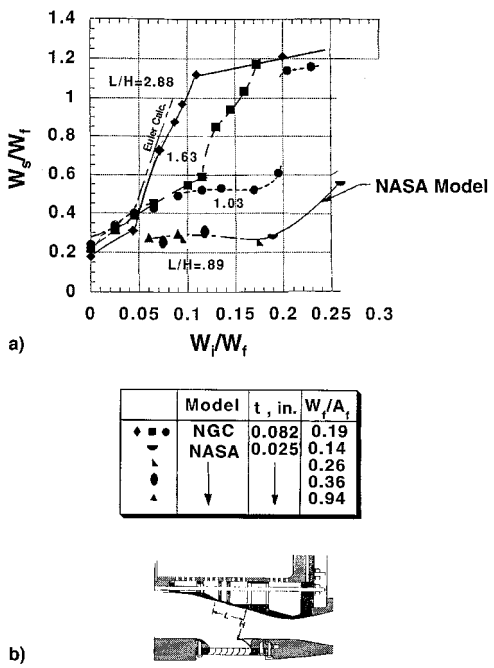

Fig. 7 Model performance comparison, injection angle $\phi = 90$ deg.

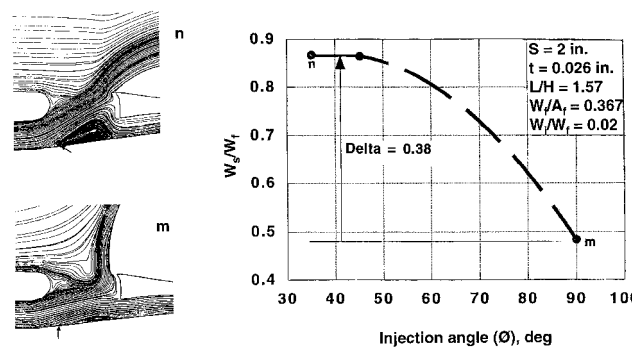

Fig. 8 Euler calculations to predict effect of injector angle.

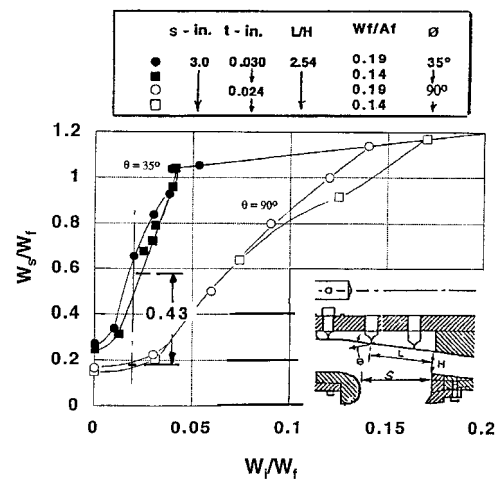

Fig. 9 Experimental results showing injection angle effects.

fan flow into the cascade opening, i.e., $W_s/W_f = 1.0$, is reduced by a factor of 3.

To verify the applicability of upstream-directed injection flow for thrust reversing, results of an evaluation of the effects of L/H for ϕ = 35-deg cases with vanes installed, are shown in Fig. 10. The upper plots show the variations of the ratio of measured reverse thrust to measured forward thrust, i.e., with reverser stowed. The lower plots show the corresponding variations in cascade-opening flow ratio. Unlike the L/H results for the ϕ = 90-deg cases of Fig. 7, wherein the largest L/H (2.88) filled the opening with the smallest injection flow, the performance of the largest L/H (2.81) in this ϕ = 35 deg case would require the largest injection flow to reach saturation, if enough data were taken. The intermediate L/H case (1.57) achieves saturation with the smallest injection flow, i.e., with $W_i/W_f = 0.025$. Note that the turning efficiency of the optimum point, described by the ratio of flow turned (fan flow) to flow required to influence the turn (injection flow), is $W_s/W_i = 37$.

Maximum reverse thrust is achieved by the $L/H = 1.57$ case, over the injection flow range $0.05 > W_i/W_f > 0.03$. At lower injection flows, the larger L/H case provides the largest reverse thrust, which deteriorates rapidly at lower injection flows. Practical concerns about controllability of reverse thrust operation may preclude the ability to operate anywhere on the very steep rate of the cascade flow–injection flow curve, i.e., prior to saturation. It may be desirable to provide the controllability inherent in operating on the relatively flat slope of the saturation line at the expense of a small increment in injection flow requirement.

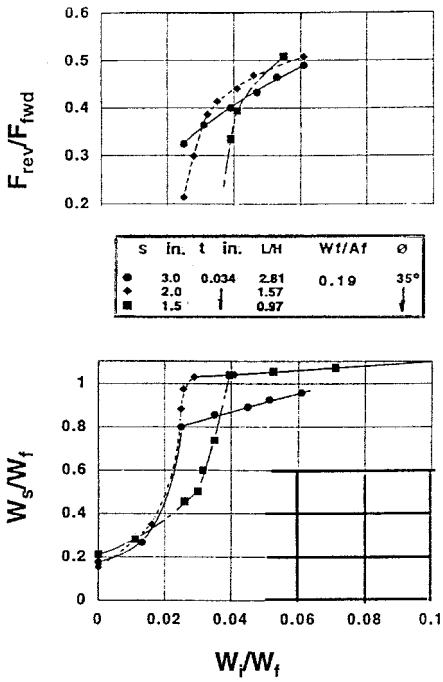

Fig. 10 Effects of cascade opening on NGC model performance.

The data of Fig. 10 have been recast by cross-plotting the thrust data with lines of constant W_i/W_f, to define the optimizing effects of L/H (Fig. 11). Also shown are the measured injection flow total pressure requirements, well within modern core engine bleed capabilities. Higher fan flows will require larger pressures. The trends of the plots suggest the possibility of trading reverse thrust levels for smaller amounts of injection flow than shown, using larger values of L/H.

Throat Injection Approach

Advantage was taken of the NASA model's unique ability to inject flow at the nozzle throat, thus providing an alternate approach for blocking/turning the fan flow into the cascade opening. The results shown in Fig. 12 are for a vanes-installed configuration with an injection angle of ϕ = 45 deg. They show several differences from the cases with injection opposite the cascade opening, i.e., the air curtain approach. First, the cascade is filled at a slower rate, i.e., more injection flow is required to achieve any level of cascade flow. Also, since the injection flow cannot be included in the reverse flow process, saturation is not possible. The maximum cascade-flow ratio achieved is $W_s/W_f = 0.80$, implying that 20% of the fan flow plus the injected flow proceeds through the nozzle and develops forward thrust. Evidently, the blockage created by the throat-blowing configuration is not as effective as the fan blockage and nozzle duct constriction of the air curtain approach. One reason for this may be that it is relatively difficult to cause the fan through-flow to separate from the nozzle walls because the generally converging character of the nozzle section imposes a favorable static pressure gradient. As with the air curtain case, a more forward-directed injection flow, as recommended by Federspiel et al.,[5] may increase cascade flow and improve reverser performance.

Performance and Operability Characteristics

The fan flow reverser effectiveness of representative configurations of both models, upstream injection with the NGC model and throat injection with the NASA model, are plotted against specific fan flow in Fig. 13a. These results are compared against the NASA model's blocker door results. The throat-blowing configuration achieved effectiveness values within the range $F_{rev}/F_{fwd} = 0.20–0.30$, requiring a nominal injection flow ratio of $W_i/W_f = 0.10$. Performance for the upstream-injection configuration, $F_{rev}/F_{fwd} = 0.40–0.45$, required a nominal injection flow ratio of $W_i/W_f = 0.05$. This level of performance compares well with the blocker door data. It should be noted that the cascade vane configurations for both models are not tailored to the approaching flowfields nor to engine operability requirements.

The back-pressure effects for the two models are compared in Fig. 13b by locating the fan-specific flow vs pressure ratio curves for the BETR configurations relative to the cascade-stowed and deployed (without blowing) cases. The NGC model results for an $W_i/W_f = 0.035$ case show a relatively small back pressure. The NASA model data show that the throat-injection results for injection flow ratios of $W_i/W_f = 0.05$ would not exceed the maximum fan pressure ratios, but that operation

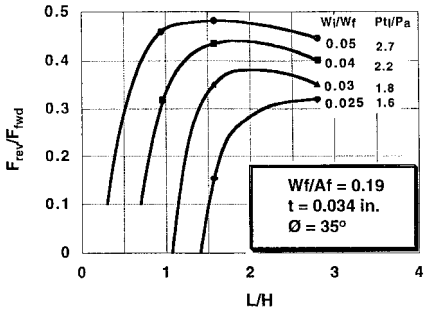

Fig. 11 Reverse thrust optimization.

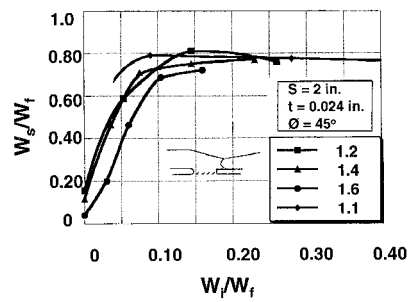

Fig. 12 NASA model performance at various FPR.

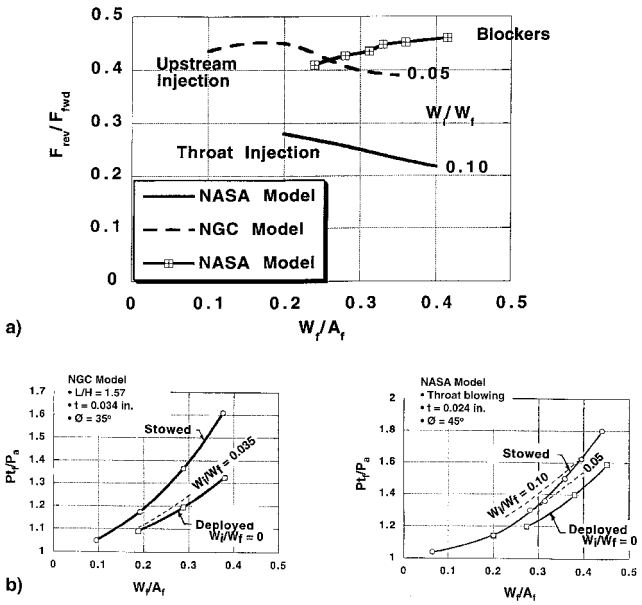

Fig. 13 Performance and operability characteristics: a) thrust performance and b) back-pressure effects.

with $W_i/W_f = > 0.10$ would. Because the thrust performance data for throat injection requires $W_i/W_f = 0.10$, fan back-pressure effects would need to be addressed in subsequent development.

Concluding Remarks

Application of a Euler analysis to guide the test progress and interpret test results was key to the relatively rapid progress that was made. The Euler analysis predicted that, and indicated why, fan flow turning performance is maximized by injecting the core bleed flow through an upstream-directed jet angle, which was verified by test data. The key appears to be the separation bubble (vortex system) produced by the interaction between jet, fan flow, and surface, which simultaneously deflects fan flow outward and constricts the downstream nozzle duct. The system behaves as a vortex valve for controlling the thrust reverser. The analysis and test results verified that all of the fan flow plus injected flow was turned into the cascade opening, with low injection flow (core bleed flow) requirements.

Testing with the NGC model has demonstrated that thrust reverser effectiveness levels in the range of 0.30–0.48 are possible with the curtain jet approach for injection flows less than $W_i/W_f = 0.05$. The throat-injection approach, evaluated by the NASA model, was not as successful, achieving lower reverse thrust performance and requiring much larger injection flows. Although the two models did not demonstrate the same degree of success, primarily because of emphasizing different areas of investigation, their results complemented and supported an understanding of the basic physics of the problem. Although no attempts have been made to accommodate engine operability issues, fan back-pressure effects appear to be less significant for the curtain jet approach than for the throat-blowing approach.

A completely optimized BETR design, i.e., the result of a systematic sweeping of S, L/H, ϕ, and t, has not been achieved to date. It is unlikely that it would have been very significant had it been achieved. Optimizing activities must await the integration of engine operability requirements that can influence cascade vane design and transcowl positioning. Also, the NGC model, being axisymmetric, is an approximation of an actual turbofan exhaust system. An actual engine installation will require consideration of effects of a discontinuous cascade opening and a varying wall thickness around the periphery. In addition, testing at landing speeds other than zero will be required and may modify some conclusions that are based on the present static test results. The Euler CFD analysis, which was done for a freestream Mach number of $M_0 = 0.10$, lends some credence to an expectation of successful forward-speed results.

Integration of a BETR with a turbofan engine will be significantly influenced by the engine bypass ratio. An injection requirement of $W_i/W_f = 0.025$, for example, will necessitate bleeding 22.5% of the total core engine flow, for a BPR = 9 turbofan engine. Because this may impact engine operability, an integrated engine manufacturer/airframer effort will be necessary to assure a viable thrust reverser design.

Acknowledgments

The authors would like to thank Scott Asbury, Michael Chen, and Barry Gilbert for their contributions to this paper. Scott Asbury and Michael Chen provided input from the NASA work. Barry Gilbert directed the Northrop Grumman/Polytechnic University experimental activities.

References

[1]Yetter, J. A., "Why Do Airlines Want and Use Thrust Reversers?" NASA TM 109158, Jan. 1995.

[2]Tindell, R., "Experimental Evaluation of the Blockerless Thrust Reverser Concept," Northrop Grumman, Rept. ATDC 95-105, April 1995.

[3]"Thrust Reverser," Societe Nationale d'Etude et de Construction de Moteurs d'Aviation, Paris, France, Publication, April 1954.

[4]Abramovich, G. N., *The Theory of Turbulent Jets*, MIT Press, Cambridge, MA, 1963, pp. 365–370.

[5]Federspiel, J., Bangert, L., Wing, D., and Hawks, T., "Fluidic Control of Nozzle Flow—Some Performance Measurements," AIAA Paper 95-2605, July 1995.